Lead-doped scintillator dosimeters for detection of ultrahigh dose-rate x-rays

Alexander Hart, Daniel Cecchi, Cloé Giguère, Frédérique Larose, François Therriault-Proulx, Nolan Esplen, Luc Beaulieu, and Magdalena Bazalova-Carter

2022

IOP Publishing Phys. Med. Biol. 67 (2022) 105007 https://doi.org/10.1088/1361-6560/ac69a5

Physics in Medicine & Biology

IPEM Institute of Physics and Engineering in Medicine

PAPER

Lead-doped scintillator dosimeters for detection of ultrahigh dose-rate x-rays

Alexander Hart[1], Daniel Cecchi[2], Cloé Giguère[3,4], Frédérique Larose[3,4], François Therriault-Proulx[5], Nolan Esplen[1], Luc Beaulieu[3,4] and Magdalena Bazalova-Carter[1]

[1] Department of Physics and Astronomy, University of Victoria, Victoria, BC, Canada
[2] Department of Physics and Astronomy, University of Calgary, Calgary, AB, Canada
[3] Departement de Radio-Oncologie et Axe oncologie du Centre de recherche du CHU de Quebec, CHU de Quebec, Quebec, QC, Canada
[4] Departement de Physique, de Genie Physique et d'Optique et Centre de Recherche sur le Cancer, Universite Laval, Quebec, QC, Canada
[5] Medscint Inc., Quebec, QC, Canada

E-mail: alexanderjhart@uvic.ca

Keywords: FLASH radiotherapy, UHDR x-rays, plastic scintillator dosimetry, kilovoltage radiotherapy

OPEN ACCESS

RECEIVED
28 October 2021

REVISED
19 March 2022

ACCEPTED FOR PUBLICATION
22 April 2022

PUBLISHED
11 May 2022

Abstract

Objective. Lead-doped scintillator dosimeters may be well suited for the dosimetry of FLASH-capable x-ray radiotherapy beams. Our study explores the dose rate dependence and temporal resolution of scintillators that makes them promising in the accurate detection of ultrahigh dose-rate (UHDR) x-rays. *Approach.* We investigated the response of scintillators with four material compositions to UHDR x-rays produced by a conventional x-ray tube. Scintillator output was measured using the HYPERSCINT-RP100 dosimetry research platform. Measurements were acquired at high frame rates (400 fps) which allowed for accurate dose measurements of sub-second radiation exposures from 1 to 100 ms. Dose-rate dependence was assessed by scaling tube current of the x-ray tube. Scintillator measurements were validated against Monte Carlo simulations of the probe geometries and UHDR x-ray system. Calibration factors converting dose-to-medium to dose-to-water were obtained from simulation data of plastic and lead-doped scintillator materials. *Main Results.* The results of this work suggest that lead-doped scintillators were dose-rate independent for UHDR x-rays from 1.1 to 40.1 Gy s^{-1} and capable of measuring conventional radiotherapy dose-rates (0.1 Gy s^{-1}) at extended distance from the x-ray focal spot. Dose-to-water measured with a 5% lead-doped scintillator detector agreed with simulations within 0.6%. *Significance.* Lead-doped scintillators may be a valuable tool for the accurate real-time dosimetry of FLASH-capable UHDR x-ray beams.

1. Introduction

Ultra-High dose-rate (UHDR) radiotherapy (RT) aims to simultaneously reduce treatment times and increase the quality of cancer treatment. By triggering the so-called FLASH effect, UHDR treatments can potentially spare damage to healthy tissue, when compared with conventional low dose-rate RT (CONV-RT), while delivering an isoeffective dose to tumours in sub-second irradiations (Favaudon *et al* 2014, Bourhis *et al* 2019, Vozenin *et al* 2019, Esplen *et al* 2020). Adoption of a UHDR treatment paradigm, in which single-fraction or hypo-fractionated FLASH-RT schedules might be conceived (Montay-Gruel *et al* 2021), could foster improved patient outcomes, by increasing the therapeutic index and freezing organ motion, while also providing opportunities to increase patient throughput in the clinic. Radiobiologists, however, do not yet fully understand the mechanisms by which UHDR radiotherapy can engage the sought after benefit of the FLASH effect (Adrian *et al* 2020, Jin *et al* 2020).

To elucidate the biological mechanisms behind FLASH, and maximally exploit the defining tissue sparing effects, it is essential that the dosimetric properties of the requisite UHDR radiation sources are characterized both accurately and reproducibly. To date, the FLASH effect has been observed with several types of particle radiation, including electrons (Montay-Gruel *et al* 2017), protons (Hughes and Parsons 2020), and heavy ions

(Kim *et al* 2021) in addition to x-rays (Montay-Gruel *et al* 2022), which will be the focus of this work. However, the ability to measure dose accurately and precisely at FLASH-compatible dose rates (often referenced as >40 Gy s^{-1}), and across various radiation modalities, remains a primary concern. Various dosimeters commonly employed to measure CONV-RT dose rates, which are on the order of 0.1 Gy s^{-1}, have been shown to be inappropriate for this task due to strong dose-rate dependencies. Examples notably include, ionization chambers and some solid state (i.e. diode) detectors, which offer online measurement capabilities that are vital to a rapid real-time UHDR beam monitoring system and can enable current cut-off under off-normal beam conditions. This is especially true for pulsed radiation sources which may employ very high dose-per-pulse, for which saturation effects can become difficult to correct, inclusive of the electron linear accelerators that are ubiquitous within the literature for FLASH-RT (Petersson *et al* 2017, Esplen *et al* 2020). As such, there yet remains a need to adapt or find new traceable reference dosimeters as well as relative dosimetry techniques that can enable dose monitoring for patient treatments, especially where active dosimetry is concerned. X-rays produced by linear accelerators for CONV-RT are routinely measured with ionization chambers and radiochromic film. Ionization chambers are commonly used as reference dosimeters with a traceable calibration and offer the capacity for online dose monitoring. Moreover, they can be successfully employed in continuous UHDR x-ray (Fournier *et al* 2016) and proton sources (Liszka *et al* 2018, Patriarca *et al* 2018) with careful application of conventional protocols (i.e. TRS 398), assuming the source may be considered continuous. Unfortunately, they also require laborious dose-rate dependent calibration factors, complicating their use for commonly used pulsed (i.e. linear accelerator) radiation sources which can produce dose rates spanning the range suitable for CONV-RT and FLASH-RT (Petersson *et al* 2017). Film, on the other hand, provides excellent spatial resolution, but lacks the temporal resolution needed for dosimetry of UHDR beams. Specifically, the response of film to ionizing radiation changes over time and generally requires careful post-irradiation redoubt procedures, and are incompatible with the real-time dosimetry needs of FLASH-RT in view of clinical translation. Nevertheless, the dose-rate independence (Jaccard *et al* 2017, Jorge *et al* 2019) of radiochromic film makes it well suited to pre-treatment dose verification and quality assurance protocols.

In contrast with the previously mentioned technologies, plastic scintillator dosimeters, which respond to ionizing radiation by emitting optical light, may be a suitable alternative for UHDR dose measurements due to their dose-rate independence and high temporal resolution (Cecchi *et al*, Beddar *et al* 1992, Archer *et al* 2019, Beddar *et al*, oct 1992). Further, the ability to read out the signal from scintillators in real-time conveys a clinical advantage over dose-integrating dosimeters by enabling online dosimetry and beam monitoring compatible with adaptive radiotherapy protocols (Archambault *et al* 2010). The relative tissue-equivalence of plastic scintillators without inorganic doping also confers a distinct advantage by circumventing the need for additional energy dependent correction factors that may complicate the calculation of dose-to-water (or tissue). This contrasts with inorganic scintillators which trade tissue-equivalence for superior radiation hardness and detection efficiency (Kharzheev 2019). While inorganic scintillators offer reduced temporal resolution compared to organic materials by an order of magnitude, they maintain fast decay times in the range of tens of nanoseconds (Kim *et al* 2021). To date, some evidence supporting the use of scintillation detectors in UHDR x-ray fields exists for point measurements in kilovoltage synchrotron beams (Archer *et al* 2019) and for proton and electron beams using various 2D detectors (Ashraf *et al* 2020). Nevertheless, plastic scintillators, while demonstrated to be excellent dosimeters for CONV-RT, must be further tested in the short time-intervals and at ultrahigh dose-rates characteristic of FLASH-RT (Debnath *et al* 2020).

In this work, we demonstrate the feasibility of using plastic scintillators and hybrid lead-doped scintillators for dosimetry of continuous, low energy (80 to 120 kVp) UHDR x-rays produced by a conventional x-ray tube equipped with a beam shutter system (Cecchi *et al*, Bazalova-Carter and Esplen 2019). Temporal resolution is assessed by measurement of sub-second irradiations and dose rate independence (i.e. linearity of response to dose rate) is investigated by measuring both UHDR and CONV-RT dose rates with the same x-ray source.

2. Materials and methods

2.1. Ultrahigh dose rate x-ray system

All irradiation experiments described in this work were conducted using an MXR-160/22 conventional x-ray tube (Comet, Flammatt, Switzerland). The x-ray tube was modified with an in-house designed, removable shutter system (figure 1), allowing samples to be placed within 2.5 cm of the x-ray focal spot and exposed to x-rays for a user-defined duration (Cecchi *et al*). The beryllium window of the x-ray tube was positioned 1.69 cm from the x-ray focal spot and recessed 0.75 mm from the face of a 2.5 mm thick tungsten shutter wheel which shielded samples from radiation exposure. The shutter wheel rotated a 1 mm wide rectangular slit using a stepper motor to allow UHDR x-rays to reach the scintillators placed in a 0.2 ml test tube (Fisher Scientific, Nepean, ON, Canada). Using this system, dose rates of 114 Gy s^{-1} to water have been achieved (Bazalova-Carter and Esplen 2019). The dose rate can be scaled by

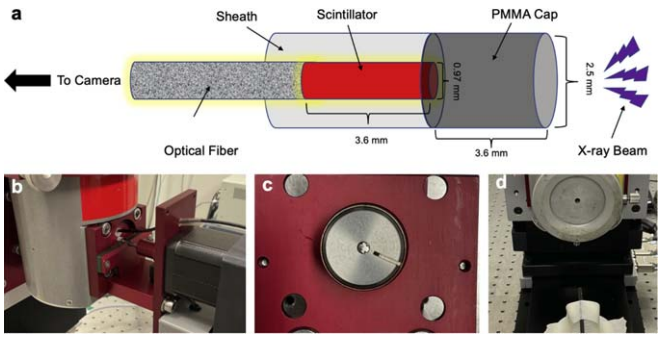

Figure 1. A schematic of the scintillator construction and orientation relative to x-rays (a). Experimental setup with a scintillator placed in the x-ray shutter system (b), with the 2.5 mm thick tungsten shutter wheel allowing x-rays to pass through the 1 mm wide slit (c). Measurements at extended SDD were taken without the shutter system in place, and a 5 mm diameter collimator shaping the beam (d).

Table 1. Material composition of scintillators by mass and their mass densities.

Probe	Composition	Density (g cm^{-3})
BCF-10	C: 92.6%, H: 7.74%	1.050
Pb 0.5%	C: 91.66%, H: 7.84%, Pb: 0.5%	1.101
Pb 1.4%	C: 90.85%, H: 7.75%, Pb: 1.4%	1.194
Pb 5%	C: 89%, H: 6%, Pb: 5%	1.562

adjusting the tube current and the total dose delivered to a sample can be specified by changing the speed of the shutter wheel.

2.2. Scintillator detectors

Four scintillators with different material compositions were used to measure light output in response to UHDR x-rays. Each of the scintillators was constructed according to the schematic shown in figure 1 and the composition detailed in table 1. The active scintillating volumes were 3.6 mm long with a diameter of 0.97 mm. A cap 3.6 mm long and 2.5 mm in diameter sealed the active volume from light contamination and protected it from physical damage. The dimensions of each of the probes were verified with x-ray images acquired using a photon-counting detector.

2.3. Scintillator measurements

In this work, scintillator response to UHDR x-rays was characterized by radiation experiments within the x-ray shutter system. Dose rate independence was evaluated by varying tube current from 1.0 to 37.5 mA at a fixed exposure setting of 50 ms. The temporal resolution of each scintillator was investigated using 80 kVp 25 mA x-rays and shutter exposure settings from 1 to 100 ms. The shutter exposure setting controls the rotational speed of the shutter wheel. Slower speeds result in longer exposures to x-rays as the 1 mm rectangular aperture sweeps across the sample holder. Energy dependence experiments were conducted by irradiating each scintillator with 80, 100, and 120 kVp tube voltages with a fixed tube current of 25 mA and a shutter exposure setting of 50 ms. Scintillator measurements outside the shutter system at source-to-detector distances (SDDs) of 10 to 20 cm were also conducted at 80 kVp, 2.5 mA, to verify the ability to measure CONV-RT dose rates. For these measurements, the 5% Pb scintillator was taped to a motion stage and the x-ray beam was shaped with a 5 mm diameter lead collimator as shown in figure 1(d).

Scintillator light output was measured using the HYPERSCINT dosimetry research platform (HYPERSCINT-RP100, Medscint, Quebec, Canada). All scintillator measurements were acquired over 5 second intervals, with a frame rate of 400 fps (2.5 ms integration time). A background reading was acquired and subtracted from measurement for each scintillator on each day of data acquisition. For all scintillator irradiation experiments, three trials were recorded.

2.4. Monte Carlo (MC) simulations

The scintillator measurements in this study were validated and normalized using MC simulations of the irradiation setup and probe geometries. Phase-space files for 80, 100, and 120 kVp tube voltages with 21.6×10^6, 26.8×10^6, and 31.6×10^6 photons, respectively, were produced with EGSnrc/BEAMnrc (Kawrakow *et al* 2000) and then used in TOPAS (Perl *et al* 2012, Faddegon *et al* 2020) to score dose within the active scintillator volume of each scintillator. The x-ray shutter system and scintillator geometries shown in figure 1 were accurately modelled within TOPAS using probe compositions listed in table 1. The components of the scintillators were modeled as described by Cecchi *et al*. The simulated probe geometry was determined using the x-ray image of the 5% Pb probe (the active scintillator was visually discernible due to the high concentration of Pb). The same probe geometry (shown in figure 1) was used for each of the scintillator material compositions. In addition to the lead-doped and plastic scintillators, a simulation of dose-to-water in the place of the scintillator material using the same probe geometry was included. For each probe, 81 shutter positions were simulated, in 0.5° steps (spanning a 40° rotation). This was repeated 10 times with unique random seeds before combining into a single simulation. Scored dose (Gy) for each shutter position was normalized by the number of initial electrons simulated in the EGSnrc simulation and then scaled by tube current to obtain dose rate (Gy s^{-1}). The duration of each shutter position was determined using the angular velocity of the stepper motor for various exposure settings.

2.5. Data analysis

For temporal dose rate profiles, the three trials acquired for each scintillator measurement were aligned using the maximum output and averaged to obtain a single dose rate profile. The measured exposure duration was determined by calculating the full width at half maximum (FWHM) for each scintillator measurement for exposure settings from 1 to 100 ms. The mean and standard deviation of the five measurements at each exposure setting were taken as the measured FWHM and error, respectively. The signal-to-noise ratio (SNR) was calculated for each scintillator according to:

$$SNR = \frac{SO_{\max}}{SO_{SD}}, \tag{1}$$

where $SO_{\max}$ is the maximum scintillator output from a 80 kVp, 25 mA, 10 ms exposure, and SO_{SD} is the standard deviation of the scintillator output from 50 frames measured with the shutter wheel blocking the beam.

For dose measurements, the mean and standard deviation of the three integrated scintillator signals were calculated as the measured dose and error, respectively. Scintillator output recorded in arbitrary units of light output was normalized using MC simulation data for each of the measured probes. For temporal dose rate profiles, scintillator output from each frame was scaled by a correction factor, *cf*, defined as:

$$cf = \frac{MC_{\max}}{SO_{\max}}, \tag{2}$$

where $MC_{\max}$ is the maximum dose rate to medium (Gy s^{-1}) calculated from simulations, and $SO_{\max}$ is the maximum scintillator output. To compare with simulation data, the measured and simulated profiles were fit with a Gaussian and aligned to their maximum output and dose rate, respectively.

For dose measurements, including dose as a function of tube current, and shutter exposure setting, scintillator output was integrated using the full width at tenth maximum (FWTM). The scintillator measurements were then normalized using the integrated FWTM dose to scintillator material (Gy) of the MC data at 80 kVp and 25 mA tube current. To assess the energy dependence and water equivalency of the probes, calibration factors from dose-to-medium to dose-to-water were calculated from simulations for each scintillator material and tube voltages of 80, 100, and 120 kVp. The calibration factor was defined as

$$\text{calibration factor} = \frac{D_W}{D_{scintillator}}, \tag{3}$$

where D_W, and $D_{scintillator}$ are the FWTM integrated doses to water and to scintillator material, respectively. The calibration factors were then validated by converting dose-to-medium to dose-to-water for scintillator measurements at each tube voltage and comparing with simulated dose-to-water. All data analysis was conducted using Python (v3.8.2).

3. Results

Figure 2 shows the measured and simulated dose rate to each scintillator as a function of exposure time for 10 ms and 100 ms shutter exposures. Each measured scintillator temporal profile matched well with MC. Measured

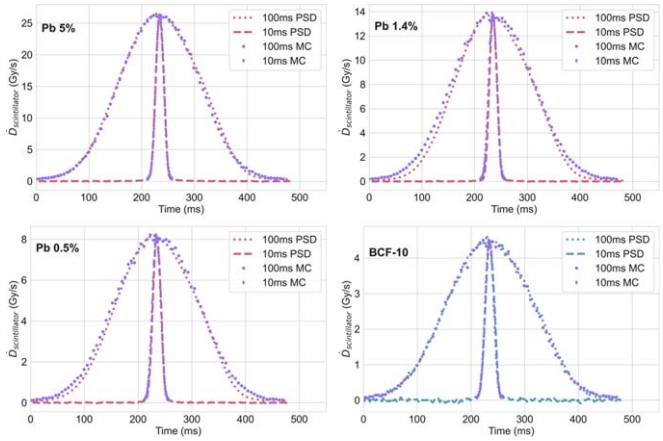

Figure 2. Dose rate to medium as a function of time for 10 and 100 ms shutter exposure settings. Measured scintillator output is shown with MC simulations for all probes for 80 kVp 25 mA x-rays.

Table 2. Measured SNR for each scintillator exposed for 100 ms to 80 kVp, 25 mA x-rays.

Scintillator	SNR
Pb 5%	1146.2
Pb 1.4%	1216.9
Pb 0.5%	670.8
BCF-10	140.3

Table 3. Maximum dose rate to medium (Gy s^{-1}) from simulation data for each scintillator composition as well as dose-to-water at 37.5 mA for 80 kVp and 25 mA for both 100 and 120 kVp.

Scintillator	80 kVp	100 kVp	120 kVp
Pb 5%	40.1	35.2	43.0
Pb 1.4%	21.2	18.1	21.0
Pb 0.5%	12.8	10.7	12.3
BCF-10	7.1	5.8	6.6
Water	14.4	11.6	13.1

SNR for each of the scintillators is listed in table 2. The lead-doped probes showed the highest SNR values, with the 1.4 and 5% probes an order of magnitude greater than the pure plastic scintillator, BCF-10.

The maximum instantaneous dose rates absorbed by the scintillators were calculated from MC simulations for each of the probe compositions and are reported in table 3. Due to the 3.6 mm attenuating cap on each of the probes, only the 5% lead-doped probe absorbed dose rates to scintillator medium above the typical 40 Gy s^{-1} UHDR threshold. By scaling tube current from 1.0 to 37.5 mA for a tube voltage of 80 kVp, maximum instantaneous dose rates of 1.1 to 40.1 Gy s^{-1} were obtained for the 5% lead-doped scintillator.

3.1. Shutter time linearity

Normalized scintillator output presented in figure 3 showed excellent agreement with simulations for each of the probes for shutter exposure settings from 1 to 100 ms. Measured dose exhibited a linear relationship with shutter setting for all probes ($R^2 > 0.9999$). The actual exposure time for a sample within the shutter system depended on the dimensions of the irradiated sample. The measured FWHM of the dose rate profiles for the scintillators exhibited a linear relationship with shutter exposure setting, as shown in figure 4.

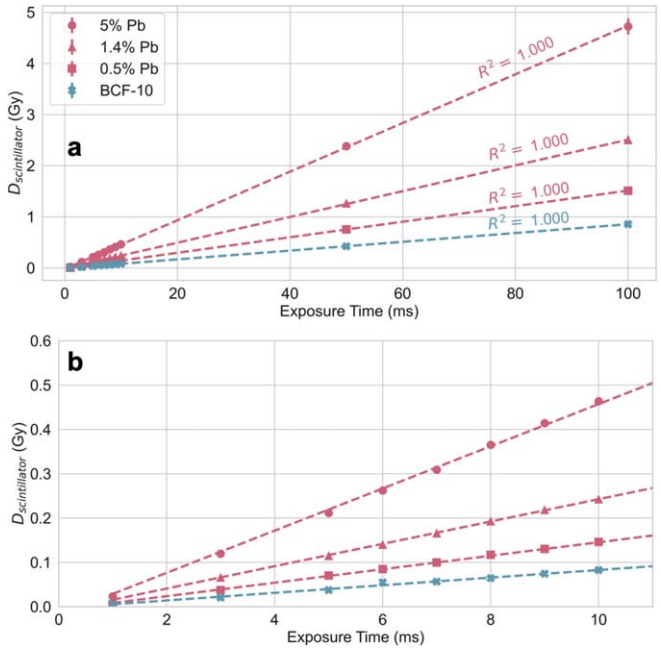

Figure 3. Dose linearity with shutter exposure setting: 1 to 100 ms (a) and 1 to 10 ms (b) for 80 kVp, 25 mA measured with all probes. The same linear fit is shown in both plots. Scintillator output was normalized to MC data for the 100 ms exposure setting.

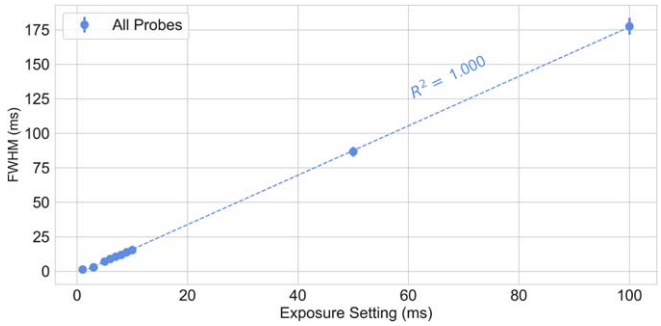

Figure 4. Measured FWHM (ms) of the scintillator output as a function of exposure setting. The average FWHM of the five scintillators is shown.

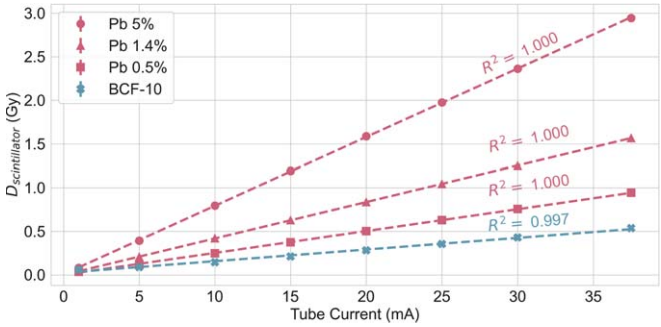

Figure 5. Dose linearity with tube current (1.0 to 37.5 mA) for 80 kVp measured with all probes. Measured scintillator output was normalized to MC data for a 50 ms exposure setting and 25 mA tube current. All scintillator measurements were taken at an exposure setting of 50 ms.

3.2. Tube current linearity

Measured dose presented in figure 5 showed a linear relationship with tube current from 1.0 to 37.5 mA for each of the four scintillators irradiated with a 50 ms exposure setting. The lead-doped scintillators demonstrated the most linear behaviour with $R^2 > 0.999$ compared to the plastic BCF-10 probe with $R^2 > 0.99$.

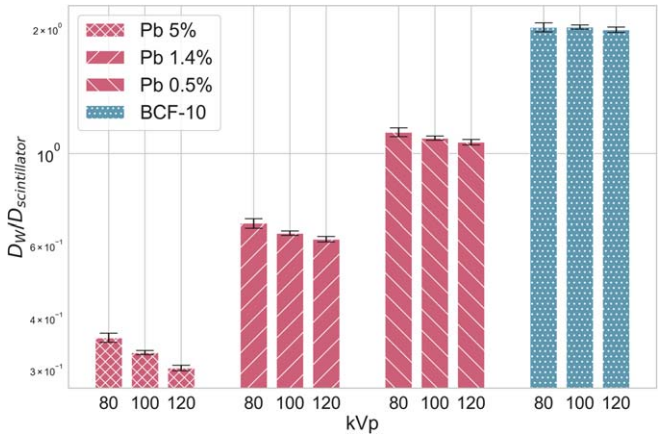

Figure 6. Water equivalency of scintillator detectors. The ratio of maximum dose rate to water to maximum dose rate to scintillator material from simulations is shown for tube voltages of 80, 100, and 120 kVp.

Table 4. Calibration factors from dose-to-medium to dose-to-water for each of the scintillator materials. The calibration factor was defined as the ratio of dose-to-water to dose to scintillator material for 80, 100, and 120 kVp tube voltages.

Scintillator	80 kVp	100 kVp	120 kVp	Mean Cal	CV
Pb 5%	0.370	0.343	0.316	0.331	6.85 %
Pb 1.4%	0.700	0.671	0.637	0.648	3.56 %
Pb 0.5%	1.159	1.126	1.091	1.094	2.28 %
BCF-10	2.059	2.038	2.008	2.013	0.68 %

3.3. Response to x-ray tube voltage

Calibration factors converting from dose-to-medium to dose-to-water are shown in table 4. The lead-doped scintillators exhibited greater energy dependence than the BCF-10 probe, with calibration factors decreasing with tube voltage. While the 0.5% Pb probe is near tissue equivalent, with a calibration factor of 1.094, the BCF-10 is the least energy dependent, with a coefficient of variation (CV) of 0.68% calculated from the three calibration factors. The energy dependence of the lead-doped probes is also evident from the ratio of maximum dose-rates shown in figure 6. Scintillator output normalized to 80 kVp MC data and converted to dose-to-water using the energy dependent calibrations factors from table 4 agreed with water simulations within 5% for the lead-doped probes, and within 8% for the undoped BCF-10. The 5% Pb probe showed the best agreement with simulations, measuring dose-to-water within 0.6% for both 100 and 120 kVp. The dose-to-water measured from each probe and percent difference from simulated dose-to-water is shown in figure 7.

3.4. Extended SDD measurements

Scintillator measurements taken outside the shutter system at increasing SDD shown in figure 8 confirmed that the dose fall-off follows an inverse square law (ISL). By reducing tube current from 25 to 2.5 mA and increasing the distance from the x-ray focal spot, CONV-RT dose rates of 0.1 Gy s^{-1} can be obtained by the 5% Pb scintillator at a tube voltage of 80 kVp.

4. Discussion

The principal aim of this investigation was to demonstrate that scintillators maintain dose rate independence and excellent temporal resolution when used to measure UHDR kilovoltage x-rays delivered in sub-second irradiations. After validating the response of each of the probes with MC simulations, we confirmed that the integrated scintillator signal captured at a frame rate of 400 fps followed a linear relationship with exposure durations of 1 to 100 ms, as shown in figure 3. All four probes exhibited dose rate independence, based on linearity of response to varying tube currents as can be seen in figure 5. While all probes were irradiated under the same conditions, because of differences in energy absorption coefficients of the different material compositions, only the 5% lead-doped scintillator absorbed dose rates reaching UHDR of 40.1 Gy s^{-1} for a tube voltage of 80 kVp and tube current of 37.5 mA.

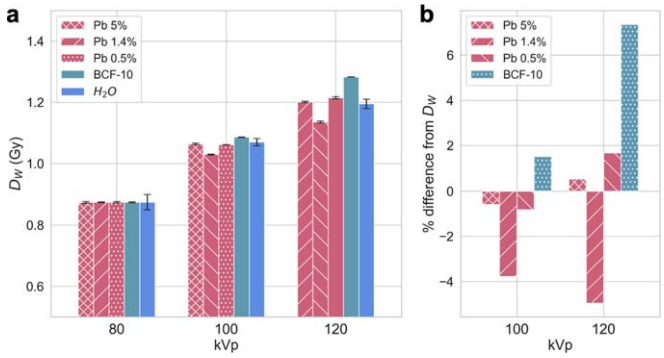

Figure 7. Measured dose-to-water for each scintillator detector, irradiated with 80, 100, and 120 kVp x-rays at a tube current of 25 mA and exposure setting of 50 ms. FWTM integrated scintillator output was normalized to dose from 80 kVp simulations for each scintillator material and then converted to dose-to-water (a). Percent difference from simulated dose-to-water is shown for measurements at 100 and 120 kVp (b).

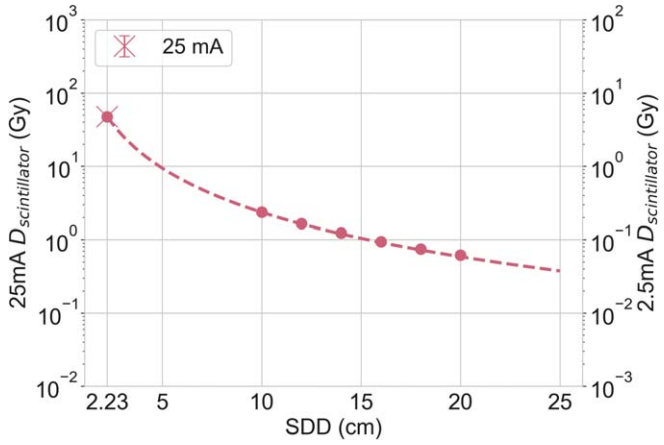

Figure 8. Integrated dose fall off at extended SDD for 80 kVp x-rays. Measured dose follows an inverse-square law relationship with distance from the x-ray focal spot. Normalized to 1 s exposure setting.

The HYPERSCINT-RP100 system used in this work is described and characterized elsewhere (Cecchi *et al*, Jean *et al* 2021, Schoepper *et al* 2022). The spectrometer is composed of an array of cooled photodetectors that collect the spectral information of the light. The signal coming from the optical fiber is therefore spread over numerous photodetectors which allows the recorded signal to be far below saturation. The light detection efficiency of the photodetector array is ~2 counts per photon across the spectral range of 400 to 700 nm according to the dosimetric characterization performed by Jean *et al* (2021). While this relatively high sensitivity could threaten saturation at ultrahigh dose-rates, this can be overcome by reducing the signal integration time and operating at high frame rates, as in this work. It is important to note that the performance characteristics of the scintillators reported in this work apply only to the combination of the scintillators and the HYPERSCINT-RP100 spectrometer together. Regarding scintillation quenching, plastic scintillators have typical response times in the ns range and therefore would not be affected by the dynamic of the beam here. Additionally, any partial dead-time would be accounted for as part of the calibration process. A continuous x-ray beam was used here and may not be subject to the same limitations as a pulsed beam.

The measurements taken at extended SDD confirmed that the unfiltered 80 kVp x-rays produced by the conventional x-ray tube in our system followed an ISL dose-rate fall off and allowed production of both UHDR and CONV-RT dose rates by adjusting tube current and distance from the x-ray focal spot. While the dose absorbed by the plastic scintillators was below the threshold for UHDR, this is due in part to the long 3.6-mm cap. The difference in μ_{en}/ρ between water and the polystyrene-based plastic scintillators (BCF-10) also results in a reduction of absorbed dose by a factor of ~2. This is confirmed by the mean calibration factor of 2.013 for BCF-10 shown in table 4. For irradiations of small biological samples, the dose rates will be >100 Gy s^{-1}, as demonstrated in previous studies of this system (Cecchi *et al*, Bazalova-Carter and Esplen 2019). This system therefore has the ability to serve as a low cost

platform for radiobiological investigations of the FLASH effect. Radiation experiments with cellular spheroids and even small animals may be conducted using this system. The use of low energy, continuous x-rays for FLASH-RT is currently an under-investigated corner of the FLASH literature.

4.1. Limitations

The lead-doped scintillators used in this work exhibited the least dose rate dependence. While this property makes lead-doped scintillators a compelling choice for UHDR dosimetry, they have the significant drawback of being non-tissue equivalent. Modifying the BCF-10 probe with a shorter cap would allow investigation of a near tissue equivalent detector at absorbed dose rates above the 40 Gy s^{-1} UHDR threshold.

The probe geometry used to simulate all probes was based on measurements from the x-ray images of the 5% Pb scintillator. However, based on the x-ray images of the 1.4% and 0.5% Pb probes, both the PMMA caps and the active scintillator volumes may be slightly shorter. This may explain the narrower temporal dose rate profiles for both 1.4% and 0.5% Pb probes compared with MC shown in figure 2. Inconsistencies in probe construction would have a significant impact on the measured SNR reported in table 2. It is expected that SNR would increase with higher concentrations of Pb, but a shorter cap could explain the higher signal measured by the 1.4% Pb probe compared to the 5% Pb probe. Also, if the PMMA cap is less than the simulated 3.6 mm, the x-ray beam would be subject to less beam hardening which could explain the under response to 100 and 120 kVp x-rays of the 1.4% Pb scintillator when normalized to 80 kVp data as shown in figure 7.

A noteworthy complication of using scintillators for dosimetry are the stem effects caused by Cherenkov radiation and radioluminescence, which must be corrected for at x-ray energies above the threshold of 178 keV (Therriault-Proulx *et al* 2013, Beddar *et al*, oct 1992). As the highest tube voltage explored in this work was 120 kVp, stem effects were not considered. However, as described by Archer *et al*, corrections must be applied when measuring higher energy sources with scintillators (Archer *et al* 2019).

The x-ray shutter system used in this work is designed to expose UHDR x-rays to a sample by rotating the 1 mm wide rectangular slit through a single point in the selected exposure time. This results in an exposure time that is dependent on the dimensions of the sample or detector placed in the test tube, which has a diameter of 6.8 mm. The actual exposure time scales linearly as our results in figure 4 show, but this design makes it more difficult to provide accurate dosimetry for samples of varying geometry. A future design which exposes the entire sample holder simultaneously could improve the usefulness of the system for more robust radiobiology studies.

5. Conclusion

This work has demonstrated that scintillators are suitable dosimeters for UHDR x-rays produced by a conventional x-ray tube. Experimental measurements with four scintillators of different material composition were compared to MC simulations. Our results confirmed that scintillator response is linear with shutter exposure setting from 1 to 100 ms and with tube current from 1.0 to 37.5 mA (corresponding to dose rates of 1.1 to 40.1 Gy s^{-1} for the 5% Pb probe). Scintillator measurements of dose-to-water agreed with simulations for tube voltages of 80, 100, and 120 kVp. Finally, by extending the source-to-detector distance and and reducing tube current, conventional dose rates of 0.1 Gy s^{-1} were measured.

Acknowledgments

We would like to thank Devon Richtsmeier for acquiring x-ray images of the scintillator probes used in this work, ensuring accurate geometries were used for the simulations. This work was partly supported by the Canada Foundation for Innovation, the British Columbia Knowledge Development Fund, NSERC Discovery Grants held by M B C and L B, an NSERC Discovery Accelerator Supplement Grant, NSERC USRA grants held by D C and C G, the New Frontiers in Research Fund, and the Canada Research Chair program.

ORCID iDs

Alexander Hart https://orcid.org/0000-0002-0547-5887
Nolan Esplen https://orcid.org/0000-0002-8347-8653

References

Adrian G, Konradsson E, Lempart M, Bäck S, Ceberg C and Petersson K 2020 The FLASH effect depends on oxygen concentration *Br. J. Radiol.* **93**
Archambault L, Briere T M, Pönisch F, Beaulieu L, Kuban D A, Lee A and Beddar S 2010 Toward a real-time *in vivo* dosimetry system using plastic scintillation detectors *Int. J. Radiat. Oncol. Biol. Phys.* **78** 280–7

Archer J, Li E, Davis J, Cameron M, Rosenfeld A and Lerch M 2019 High spatial resolution scintillator dosimetry of synchrotron microbeams *Sci. Rep.* **9** 1–7
Ashraf M R, Rahman M, Zhang R, Williams B B, Gladstone D J, Pogue B W and Bruza P 2020 Dosimetry for FLASH radiotherapy: a review of tools and the role of radioluminescence and cherenkov emission *Front. Phys.* **8** 1–20
Bazalova-Carter M and Esplen N 2019 On the capabilities of conventional x-ray tubes to deliver ultra-high (FLASH) dose rates *Med. Phys.* **46** 5690–5
Beddar A S, Mackie T R and Attix F H 1992 Water-equivalent plastic scintillation detectors for high-energy beam dosimetry: I. Physical characteristics and theoretical considerations *Phys. Med. Biol.* **37** 1883–900
Beddar A S, Mackie T R and Attix F H 1992 Water-equivalent plastic scintillation detectors for high-energy beam dosimetry: II. Properties and measurements *Phys. Med. Biol.* **37** 1901–13
Bourhis J *et al* 2019 Treatment of a first patient with FLASH-radiotherapy *Radiother. Oncol.* **139** 18–22
Cecchi D D, Therriault-Proulx F, Lambert-Girard S, Hart A, Macdonald A, Pfleger M, Lenckowski M and Bazalova-Carter M 2021 Characterization of an x-ray tube-based ultrahigh dose-rate system for *in vitro* irradiations *Med. Phys.* **48** 7399– 409
Debnath S B C, Fauquet C, Tallet A, Goncalves A, Lavandier S, Jandard F, Tonneau D and Darreon J 2020 High spatial resolution inorganic scintillator detector for high-energy x-ray beam at small field irradiation *Med. Phys.* **47** 1364–71
Esplen N, Mendonca M S and Bazalova-Carter M 2020 Physics and biology of ultrahigh dose-rate (FLASH) radiotherapy: a topical review *Phys. Med. Biol.* **65** 23TR03
Faddegon B, Ramos-Mendez J, Schuemann J, McNamara A, Shin J, Perl J and Paganetti H 2020 The TOPAS tool for particle simulation, a monte carlo simulation tool for physics, biology and clinical research *Phys. Med.* **72** 114–21
Favaudon V *et al* 2014 Ultrahigh dose-rate flash irradiation increases the differential response between normal and tumor tissue in mice *Sci. Transl. Med.* **6** 245ra93–245ra93
Fournier P, Crosbie J C, Cornelius I, Berkvens P, Donzelli M, Clavel A H, Rosenfeld A B, Petasecca M, Lerch M L F and Bräuer-Krisch E 2016 Absorbed dose-to-water protocol applied to synchrotron-generated x-rays at very high dose rates *Phys. Med. Biol.* **61** N349–61
Hughes J R and Parsons J L 2020 Flash radiotherapy: current knowledge and future insights using proton-beam therapy *Int. J. Mol. Sci.* **21** 1–14
Jaccard M, Petersson K, Buchillier T, Germond J F, Durán M T, Vozenin M C, Bourhis J, Bochud F O and Bailat C 2017 High dose-per-pulse electron beam dosimetry: usability and dose-rate independence of EBT3 Gafchromic films *Med. Phys.* **44** 725–35
Jean E, Therriault-Proulx F and Beaulieu L 2021 Comparative optic and dosimetric characterization of the HYPERSCINT scintillation dosimetry research platform for multipoint applications *Phys. Med. Biol.* **66** 085009
Jin J Y, Gu A, Wang W, Oleinick N L, Machtay M and Ming (Spring) Kong F 2020 Ultra-high dose rate effect on circulating immune cells: a potential mechanism for FLASH effect? *Radiother. Oncol.* **149** 55–62
Jorge P G *et al* 2019 Dosimetric and preparation procedures for irradiating biological models with pulsed electron beam at ultra-high dose-rate *Radiother. Oncol.* **139** 34–9
Kawrakow I, Rogers D W O, Mainegra-Hing E, Tessier F, Townson R W and Walters B R B 2000 Egsnrc toolkit for monte carlo simulation of ionizing radiation transport [release v2021] (https://doi.org/10.4224/40001303)
Kharzheev Y N 2019 Radiation hardness of scintillation detectors based on organic plastic scintillators and optical fibers *Phys. Part. Nucl.* **50** 42–76
Kim C, Lee W, Melis A, Elmughrabi A, Lee K and Park C 2021 A review of inorganic scintillation crystals for extreme environments *Crystals* **11** 669
Kim M M, Darafsheh A, Schuemann J, Dokic I, Lundh O, Zhao T, Ramos-Mendez J, Dong L and Petersson K 2021 Development of Ultra-High Dose Rate (FLASH) Particle Therapy *IEEE Trans. Radiat. Plasma Med. Sci.* **7311** 1–12
Liszka M, Stolarczyk L, Kłodowska M, Kozera A, Krzempek D, Mojzeszek N, Pędracka A, Waligórski M P R and Olko P 2018 Ion recombination and polarity correction factors for a plane-parallel ionization chamber in a proton scanning beam *Med. Phys.* **45** 391–401
Montay-Gruel P, Corde S, Laissue J A and Bazalova-Carter M 2022 Flash radiotherapy with photon beams *Med. Phys.* **49** 2055–67
Montay-Gruel P *et al* 2017 Irradiation in a flash: unique sparing of memory in mice after whole brain irradiation with dose rates above 100 Gy s^{-1} *Radiother. Oncol.* **124** 365–9
Montay-Gruel P *et al* 2021 Hypofractionated FLASH-RT as an effective treatment against glioblastoma that reduces neurocognitive side effects in mice *Clin. Cancer Res.* **27** 775–84
Patriarca A *et al* 2018 Experimental set-up for flash proton irradiation of small animals using a clinical system *Int. J. Radiat. Oncol. Biol. Phys.* **102** 619–26
Perl J, Shin J, Schumann J, Faddegon B and Paganetti H 2012 TOPAS: an innovative proton Monte Carlo platform for research and clinical applications *Med. Phys.* **39** 6818–37
Petersson K, Jaccard M, Germond J F, Buchillier T, Bochud F, Bourhis J, Vozenin M C and Bailat C 2017 High dose-per-pulse electron beam dosimetry -A model to correct for the ion recombination in the advanced markus ionization chamber *Med. Phys.* **44** 1157–67
Schoepper I, Dieterich S, Trestrail E A and Kent M S 2022 Pre-clinical and clinical evaluation of the HYPERSCINT plastic scintillation dosimetry research platform for in vivo dosimetry during radiotherapy *J. Appl. Clin. Med. Phys.* **23** e13551
Therriault-Proulx F, Beaulieu L, Archambault L and Beddar S 2013 On the nature of the light produced within PMMA optical light guides in scintillation fiber-optic dosimetry *Phys. Med. Biol.* **58** 2073–84
Vozenin M C, Hendry J H and Limoli C L 2019 Biological benefits of ultra-high dose rate flash radiotherapy: sleeping beauty awoken *Clin. Oncol.* **31** 407–15